Second International Symposium on Marine Propulsors
smp'11, Hamburg, Germany, June 2011

Loads Acting on a Semi-Spade Rudder

Andreas Brehm[1], Volker Bertram[1], Ould El Moctar[1, 2]

[1] FutureShip GmbH – A GL company, Hamburg, Germany
[2]Universität Duisburg-Essen (UDE), Duisburg, Germany

ABSTRACT

This paper presents results of a research project wherein the hydrodynamic loads acting on a semi-spade rudder of an 8.500 TEU container vessel were investigated. RANSE[1] based CFD[2] simulations were carried out and compared to full-scale and model-scale measurements. Rudder cavitation prediction and a new rudder design to minimise cavitation appearance was a main topic of the project. The influence of cavitation and free-surface modelling on the pressure distribution, and therefore on the acting forces and moments was investigated. Comparisons with measurements show that numerical fluid and structure computations could be well used to design and predict the loads acting on semi-spade rudders.

Keywords

Semi-Spade Rudder, Hydrodynamic Loads, Cavitation

1 INTRODUCTION

At the end of the last and the beginning of the new century, the speeds of various ship types as well as the propeller loadings had been increased. This had led to higher structural loads and increased cavitation on rudders. As a response to the increase in reported rudder damage on large container vessels, Germanischer Lloyd (GL) initiated a research project in 2005 focussed on the hydrodynamics of semi-balanced rudders. The main findings of this research project are presented in this paper.

2 RESEARCH PROJECT

The research project, jointly conducted with SVA Potsdam, was funded by the German Federal Ministry of Economics and Technology. The project's aims were to:

- investigate the hydrodynamics and structural loads on a large semi-balanced rudder, and
- investigate the cavitation risks and how moderate modifications may reduce cavitation occurrence.

SVA Potsdam conducted a series of model tests within the project. GL contributed its simulation experience: first, the hydrodynamic loads were computed in a RANSE approach; then, for selected cases, the loads were applied to a finite element analysis (FEA) model and the structural response of the rudder was computed. Based on the insight gained, a new rudder design with significantly reduced cavitation was developed.

We used full-scale measured rudder loads and cavitation observations to validate model test and simulation results. The test case was an 8.500 TEU container vessel, see Table 1. Towards the end of the construction phase, measuring devices to record the rudder loads and four windows to observe in-service cavitation were installed.

Table 1: Main data of investigated ship

Ship		
Length	L	> 300 m
Breadth	B	≈ 40 m
Draft	T	≈ 13 m
Design Speed	v	≈ 25 kn
Power	P	≈ 70.000 kW
Propeller		
Diameter	D_P	≈ 9 m
Number of blades	z	= 6
Rudder		
Type	Semi-spade	
Projected Rudder Blade Area	A_{RB}	≈ 75 m²
Projected Rudder Horn Area	A_{RH}	≈ 20 m²

3 VALIDATION

Numerous publications have shown the suitability of RANSE simulations for hull, rudder and propeller flows (Abdel-Maksoud et al 1998, Azcueta 2001, Streckwall et al 2001, El Moctar 1997, 2001, 2002, 2004, Heinke et al 2004, Simonsen et al 2005, Hamann et al 2007, Brehm et al 2007, 2009). Nevertheless, we conducted initial studies for our test case and our RANSE method to investigate the influence of boundary conditions and computational control parameters on results.

3.1 Model-scale case

Steady RANSE simulations for the propeller in uniform flow were compared to model tests in an open-water diagram, see Fig. 1.

[1] Reynolds Averaged Navier-Stokes Equations
[2] Computational Fluid Dynamics

The rudder was investigated in uniform flow for angles varying between 0° and 35° in steps of 5°. Figs. 2 and 3 compare measured drag and lift coefficients.

For this case, there were also model test results of the Hamburg Ship Model Basin (HSVA). The measured values differ between the two basins despite using the same model. The RANSE results lie mostly between the two measurements. Fig. 2 shows results from steady and unsteady RANSE simulations. Fig. 3 shows the transient RANSE results for the lift on the rudder blade alone and on rudder blade and rudder horn. The forces on the rudder horn cannot be measured in model tests. Therefore all other figures compare only the forces on the rudder blade.

SVA Potsdam also conducted RANSE simulations for the rudder in uniform flow. The results are included in the figures.

Of the many model tests performed, we discuss here only the measurement of the velocity field behind hull-propeller and rudder in greater detail. SVA Potsdam employed particle image velocimetry (PIV). For the model test campaign, the PIV system was enhanced by a stereoscopic camera allowing measurements of all three velocity components in one plane.

The velocity field was measured near the rudder while the ship model was towed with freely rotating propeller at drift angles of 0° and 10° and various rudder angles. There were two measurement campaigns. In the first measurement campaign, four cross-section planes were defined. One plane was between propeller and rudder, and the other three planes behind the rudder, see Fig. 4. For the second measurement campaign, a total of 28 planes were investigated.

Figs. 5 to 10 compare exemplarily RANSE simulations and PIV measurements for the measuring plane E1 for rudder angles +20°, 0° and -20°. The velocity component u (in longitudinal direction) was normalised with ship speed u_a. The agreement between simulations and model tests was generally good.

3.2 Full-scale case

The grid for the RANSE simulations covered hull, rudder and propeller. The conditions were taken as recorded during the maiden voyage of the vessel. The model was detailed enough to include all attachments to the rudder, such as baffle plates and wedges. Fig. 11 compares the cavitation extent as computed and as observed in full scale.

The torsion and bending stresses at ship's rudder stock and horn were recorded by stress-strain gauges. The FEA model was calibrated to the measuring system while the vessel was dry docked, by applying a tensile force on the rudder and measuring the stresses. The hydrodynamic loads were determined in RANSE simulations. The RANSE model covered hull, propeller and rudder and used full-scale Reynolds numbers. The following simplifications were applied:

- No free surface deformation; instead a static water column was imposed at the stern.
- No ship hull motions
- No cavitation model
- No change in propeller rpm

The rudder was kept fixed at a given rudder angle, varying between 0° and 35° in 5° steps. The periodical loads at steps of 10° propeller turn were mapped to the FEA model to compute the resulting stresses in the rudder at the positions of the stress-strain gauges. The computed stresses agreed satisfactorily with the full-scale measured stresses, see Fig. 12.

Fig. 13 shows the FEA model used and the location of the highest stresses.

The red lines in Fig. 14 show the time history of the rudder stock moment and the rudder angle during a 35/35° zig-zag sea trial. The black lines show the time histories of the RANSE simulation. The simulation neglected ship motions, cavitation, free-surface deformation and the change in propeller rpm. The rudder was moved with the same rate of turn as observed in the sea trial. The time histories of the rudder stock moment are similar between sea trial and simulation, as long as the ship has not started to turn. Then the moment histories start to diverge. The most important factor for this divergence should lie in the neglected ship motions. Cavitation, change in propeller rpm and free surface should play a minor role in this case. Further detailed studies to quantify the effects of the assorted simplifications are planned for 2011.

4 LOW-CAVITATION RUDDER DESIGN

Another goal of the project was the design of a rudder with significantly lower cavitation. A constraint for the new design was that only small modifications of the original rudder design were permitted, excluding specifically a change of rudder type (full-spade instead of semi-spade rudder), twisted rudder, a shift of the horizontal gap between horn and blade, a change of the rudder area or shift of the rudder stock. The remaining design freedom was limited to changes in the profile shape and addition of small appendages. The design was guided by 2D and 3D RANSE simulations.

In a first step, the original rudder was cut in three horizontals planes, see Fig. 15. The original full profile section in the cut A-A was investigated and improved using the potential flow code XFOIL (Drela et al 2006). The section was compared with assorted NACA profiles and hybrid profile shapes stemming from previous SVA Potsdam investigations (Heinke et al 2004). Then we designed our own profile shape aiming at a small low-pressure peak and a rather balanced pressure distribution over the chord of the profile (Fig. 16), while not making lift and drag coefficients worse.

The partition between horn and rudder for cuts B-B and C-C leads to flow phenomena that cannot be captured by XFOIL. Therefore, 2D RANSE simulations had to be

employed for these cuts. 28 gap variants were investigated. Rudder angles were varied between ±8° and angles of attack between 6° and 28° in steps of 2°. In total, more than 3000 RANSE simulations were performed.

Streamlines were used for better assessment of gap variants, see Fig. 17. Near the wall at the leading edge, particles were selected and their paths visualised in order to see whether the particles would enter the gap or not. Increased flow through the gap means increased danger of cavitation at the gap.

Based on the best 2D profile sections, a 3D model was created and investigated. The RANSE simulations included hull and propeller in the model. Only such comprehensive models can capture appropriately the 3D flow effects, which are vital for the correct assessment of forces and moments at the rudder. Details of the rudder sole have a significant impact on the rudder forces. The first design (variant A) had a significantly curved forward part, see Fig. 18. This noticeably reduced the cavitation on the rudder blade. The low pressure gradient with smooth transition between pressure and suction side unfortunately also leads to lower lift forces on the profile and therefore made variant A not acceptable.

Two further variants of the rudder sole were investigated: Variant B had a curved forward part with much smaller radius, variant C was fitted with an end plate instead of rounding the forward part, see Fig. 18.

Rudder sole cavitation is induced by low-pressure regions stemming from the fluid's attempt to balance the pressure difference between suction and pressure side by flowing rapidly from one side to the other over the sole. The broad end plate in variant C forces the major part of the flow around the leading edge which was designed to be particularly smooth to reduce cavitation. The end plate also moderates the pressure regions from the rudder surface to the outer edges of the plate on both sides. The pressure difference is then balanced at the edges with lower risk of cavitation, see Fig. 19.

Figs. 20 and 22 show the computed cavitation extent for rudder angle 5° and 10° for original rudder and our new design. The cavitation extent is significantly lower at blade and vertical gaps in our new design. Cavitation is not completely avoidable, due to the high velocities involved. For our new design, significant cavitation appears for rudder angles above 8°. However, most of the time, rudder angles do not exceed 5° in real ship operations.

For the new design, one constraint was that the lift forces should not be lower than in the original design. This condition was met, see Fig. 21. In fact, the lift forces were improved: the original rudder featured a lift force of 278 kN at 0° rudder angle, while the new design featured only 12 kN. The new design was also better in terms of rudder stock moments, see Fig. 23 While required stock moment is higher between 0° to 20°, the maximum stock moment is less than half of that of the original rudder. As the maximum stock moment determines the size of the rudder engine, this improvement has significant impact in practice.

5 CONCLUSION

In the course of the presented research project, a numerical procedure to calculate the hydrodynamic and structural behaviour of semi-spade rudders has been established. By including hull and propeller in the numerical model, the flow around the rudder was captured very realistically. Extensive model-scale and full-scale tests allowed a successful validation of the procedure.

Based on the original rudder, a new design with significantly lower cavitation risk was developed.

Generally, numerical flow and structural analyses proved to be powerful tools to support rudder design.

REFERENCES

Abdel-Maksoud, M., Menter F. R. & Wuttke, H. (1998). 'Viscous flow simulations for conventional and high skew propellers'. Ship Technology Research **45**.

Azcueta, R. (2001). Computation of Turbulent Free-Surface Flows Around Ships and Floating Bodies. PhD Thesis, Technische Universität Hamburg-Harburg.

Brehm, A. et al. (2007). 'Berechnung von örtlich auftretenden Extremlasten unter realistischen Bedingungen (RELAX)'. BMBF-Report **03SX197A**, Technische Informationsbibliothek, Hannover.

Brehm, A. et al. (2009). 'Hydrodynamische und strukturmechanische Untersuchung von Rudern großer, schneller Schiffe (XXL-Ruder)'. BMWI-Report **03SX213A**, Technische Informations-bibliothek, Hannover.

Drela, M. et al. (2006). 'XFOIL, Version 6.96'. http://web.mit.edu/drela/Public/web/xfoil/, Massachusetts Institute of Technology.

El Moctar, O. (1997). 'Berechnung von Ruderkräften'. Institut für Schiffbau der Universität Hamburg Bericht **582**.

El Moctar, O. (2001). 'Numerische Berechnung von Strömungskräften beim Manövrieren von Schiffen'. Technische Universität Hamburg-Harburg Bericht **611**.

El Moctar, O. & Lindenau, O. (2002). 'Kavitationsgefahr bei Hydroprofilen'. HANSA **10**.

El Moctar, O. (2004). 'Numerical Prediction of Hydrodynamic loads on rudders'. HANSA **7**.

Hamann et al. (2007). 'Entwicklung einer bruchmech-anischen Prozedur (ProRepaS)'. BMBF-Report **03SX209A**, Technische Informationsbibliothek, Hannover.

Heinke et al. (2004). 'Kavitationsarme Profile für Hochleistungsruder'. BMWI-Report, Vorhaben **233** (03), Schiffbau- Versuchsanstalt Potsdam.

Simonsen, Claus D. & Stern, F. (2005). 'RANS Manoeuvring Simulation of Esso Osaka with Rudder and Body-Force Propeller'. Journal of Ship Research **49**(2), pp. 98–120.

Streckwall, H. & El Moctar, O. (2001). 'RANS Simulations for Hull, Propeller and Rudder Interactions'. 4th Numerical Towing Tank Symposium, Hamburg, Germany.

FIGURES

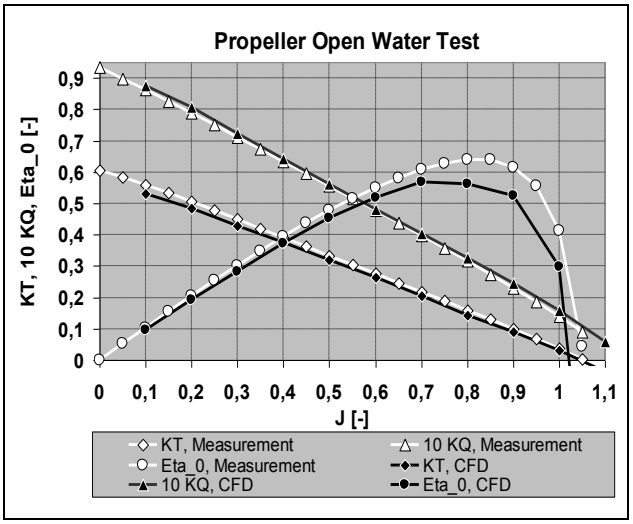

Figure 1: Calculated and measured open-water diagram

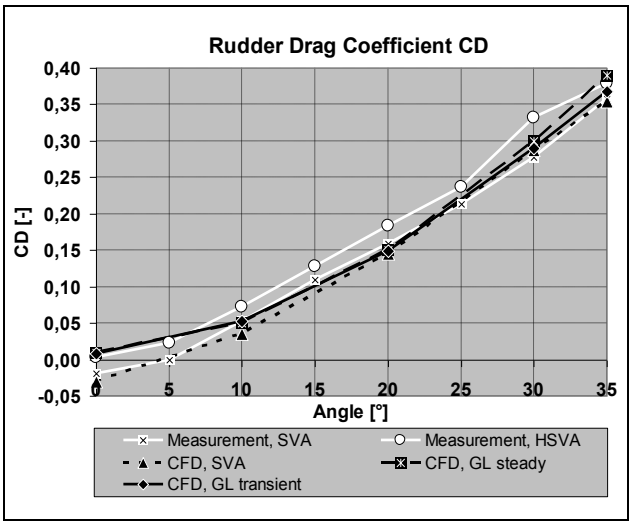

Figure 2: Calculated and measured rudder drag

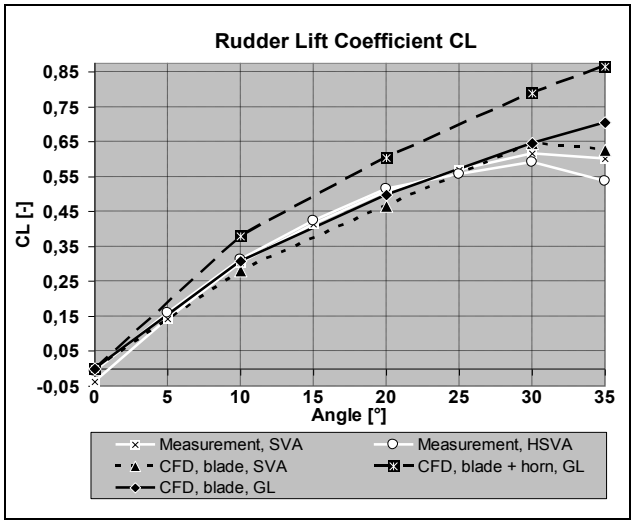

Figure 3: Calculated and measured rudder lift

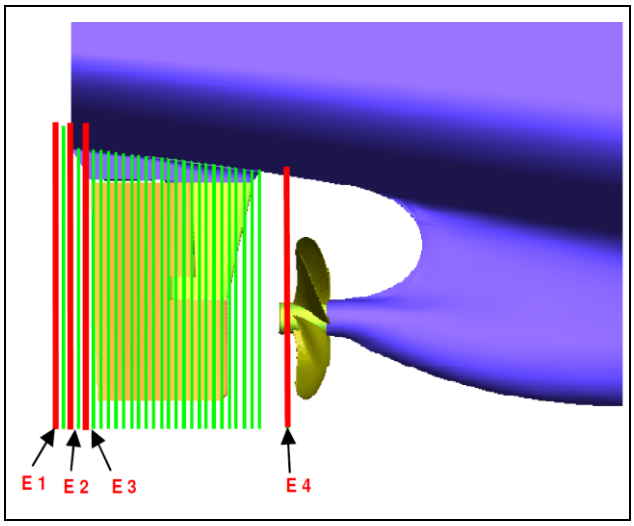

Figure 4: Locations of cross-sectional planes

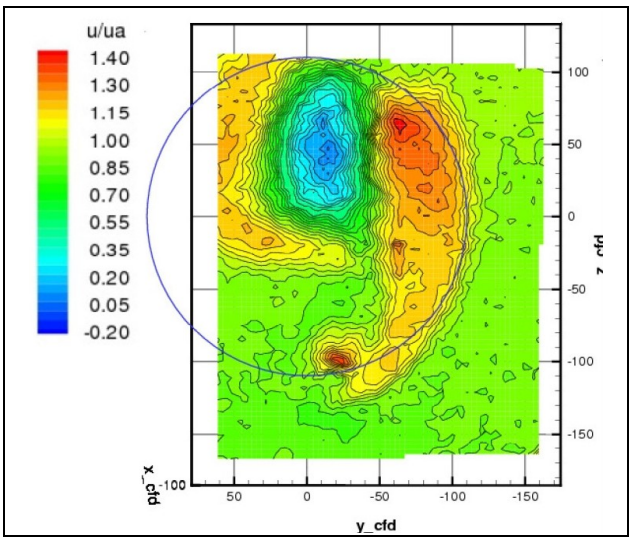

Figure 5: Measured velocities in ship's longitudinal direction in plane E1; rudder angle= +20°

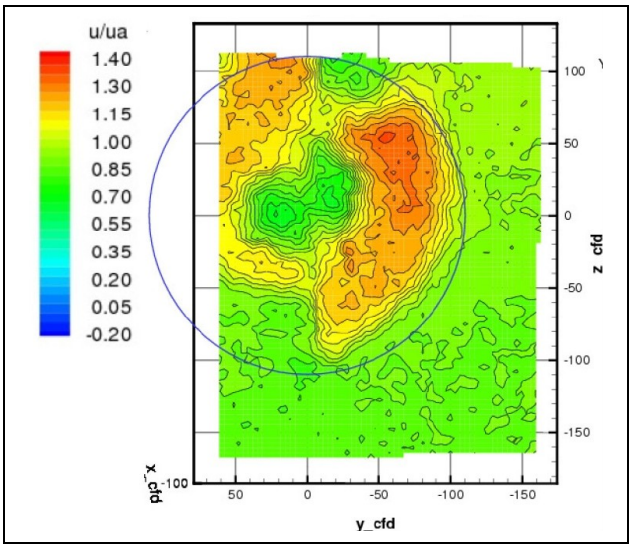

Figure 6: Measured velocities in ship's longitudinal direction in plane E1; rudder angle= 0°

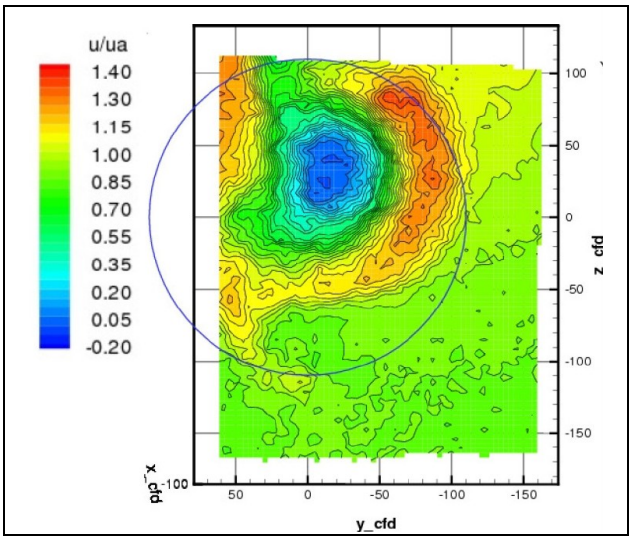

Figure 7: Measured velocities in ship's longitudinal direction in plane E1; rudder angle= -20

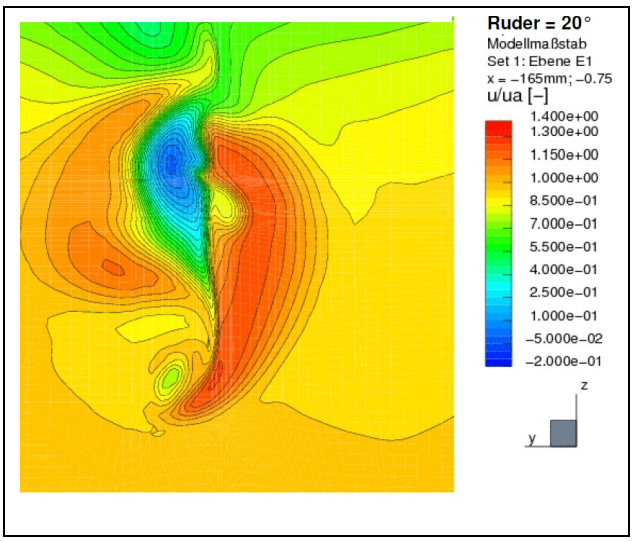

Figure 8: As Figure 5, but computed

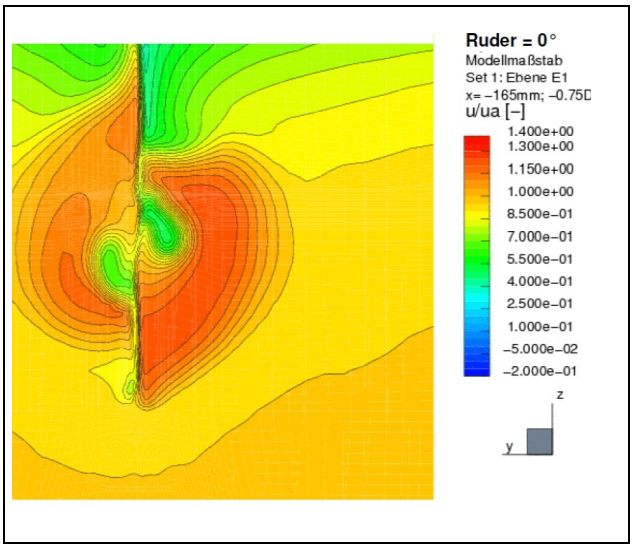

Figure 9: As Figure 6, but computed

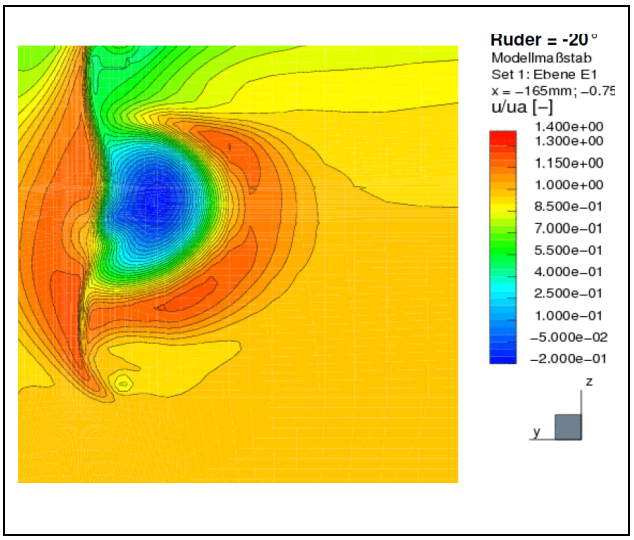

Figure 10: As Figure 7, but computed

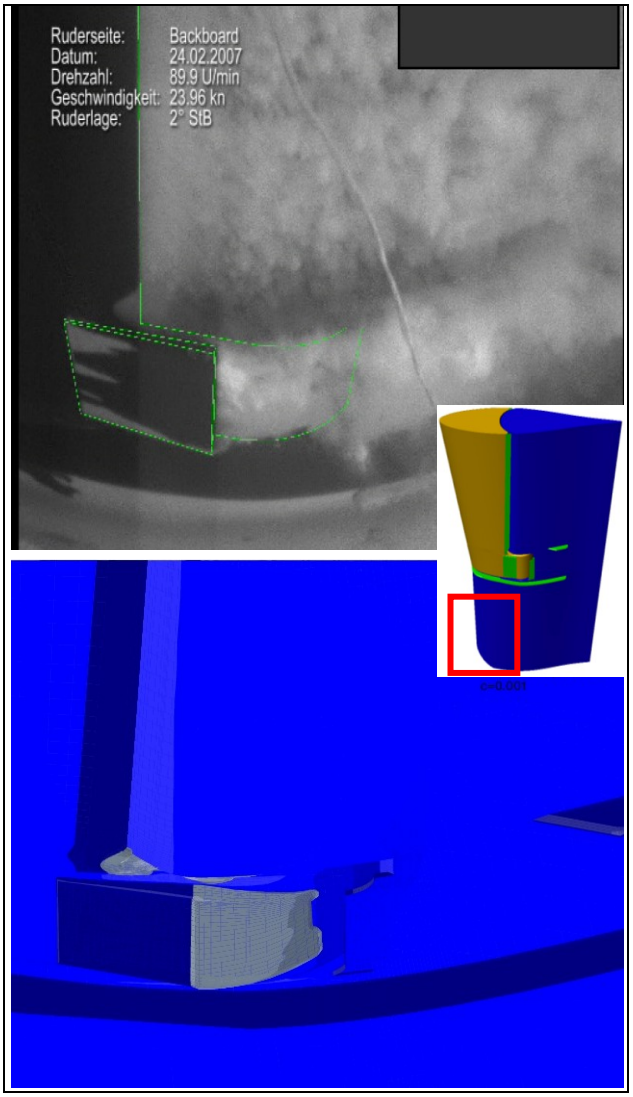

Figure 11: Cavitation clouds in full-scale observations (top) and computed iso-surface with concentration of c=0.001 water vapour (bottom)

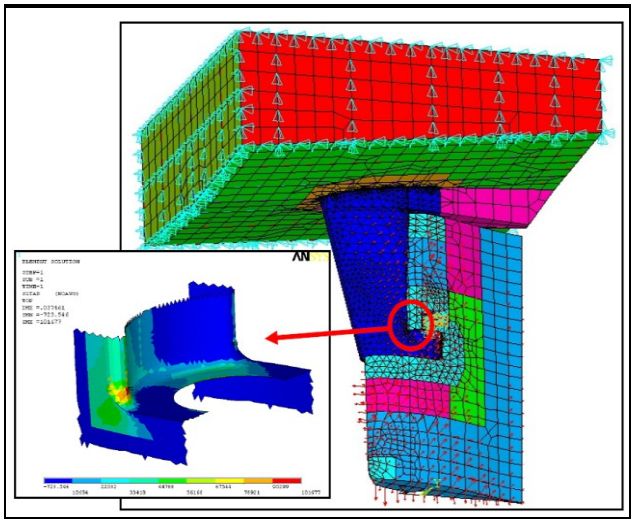

Figure 13: FEA model (right) and location with highest computed stress (left)

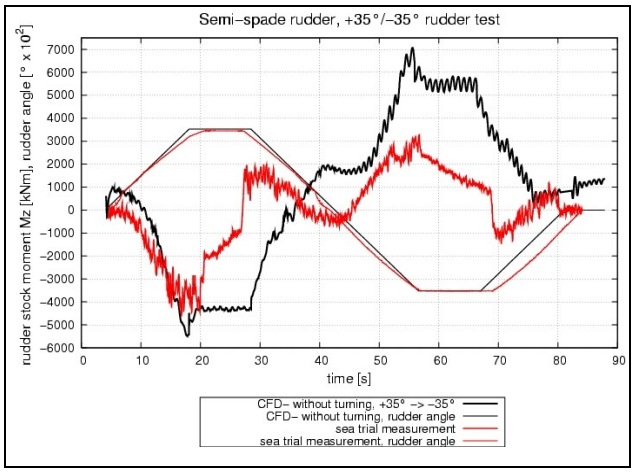

Figure 14: Time histories of full-scale measured (red) and computed (black) rudder stock moments

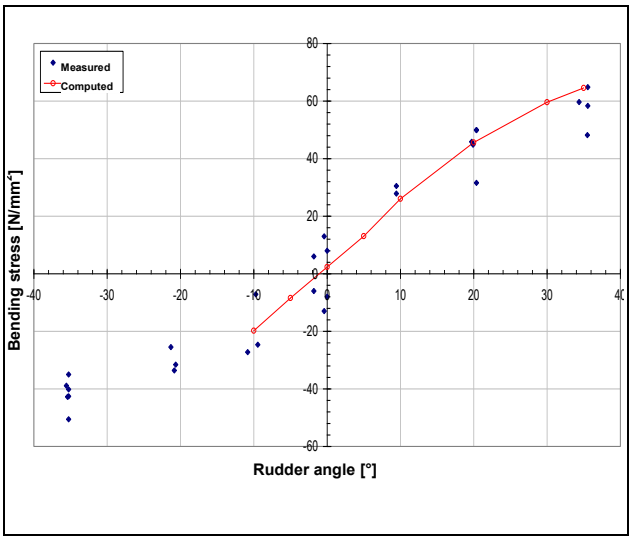

Figure 12: Computed (red line) and measured (blue dots) max. bending stress of rudder stock

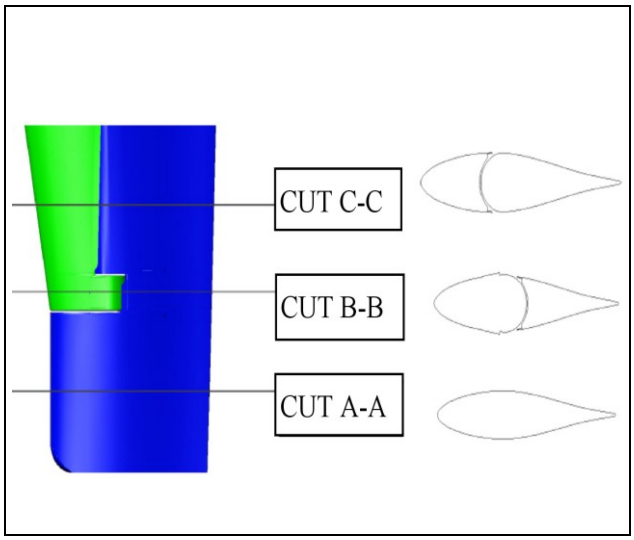

Figure 15: 2D- investigated horizontal cuts

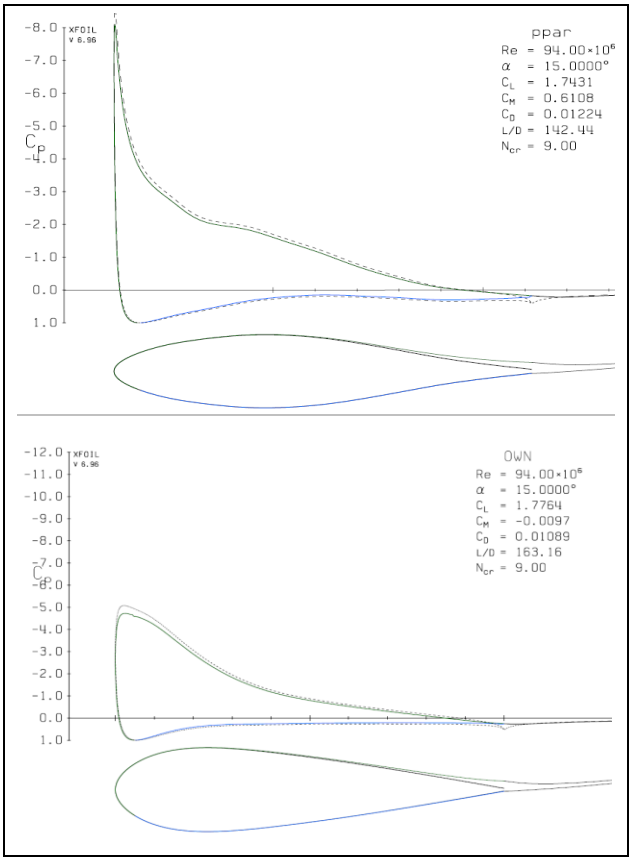

Figure 16: 2D- investigations with XFOIL: Run of the pressure coefficient across the original profile (top) and across one of the profile variations (bottom)

Figure 17: Streamlines of particles in the area of a gap; original profile (top) and a profile variation (bottom)

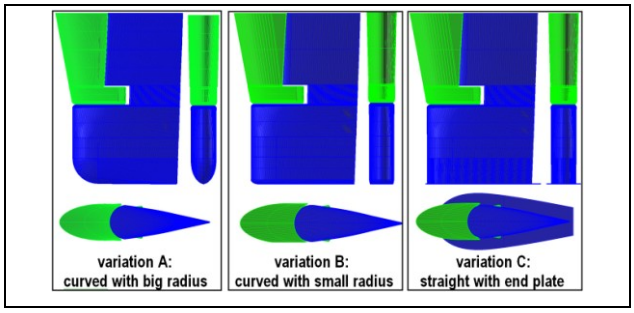

Figure 18: Geometrical variations of rudder sole

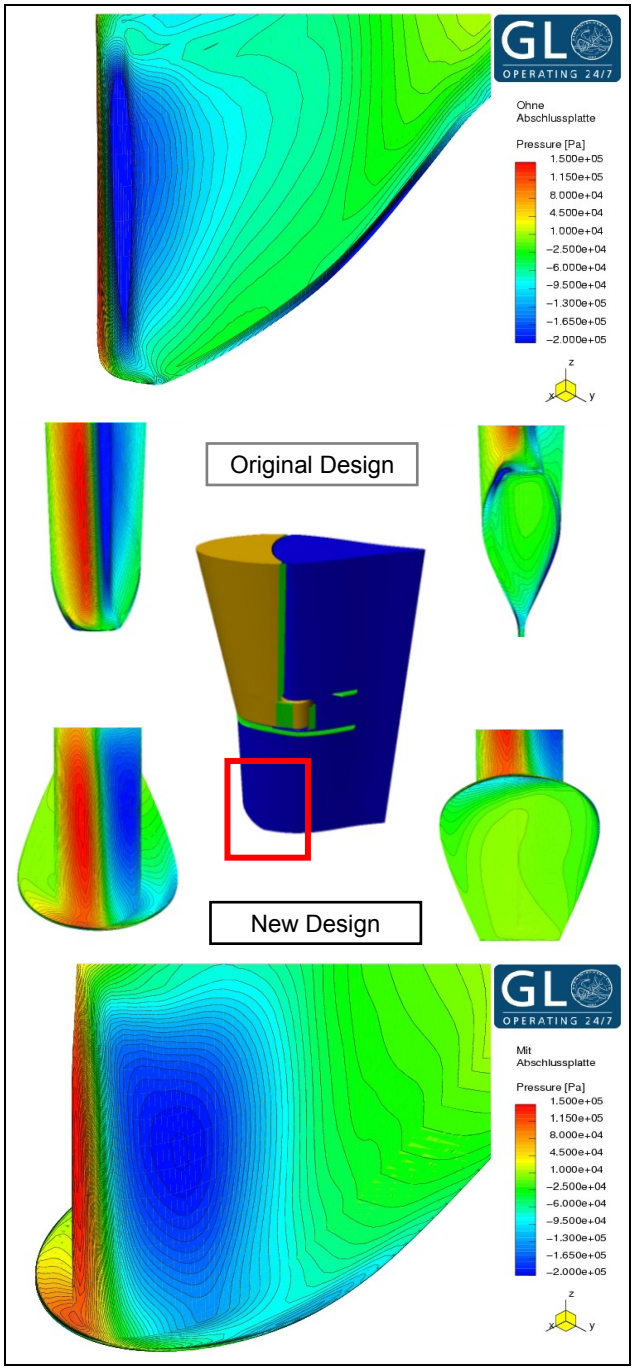

Figure 19: Pressure distribution around rudder sole of original rudder design (top) and around new design with end plate (bottom)

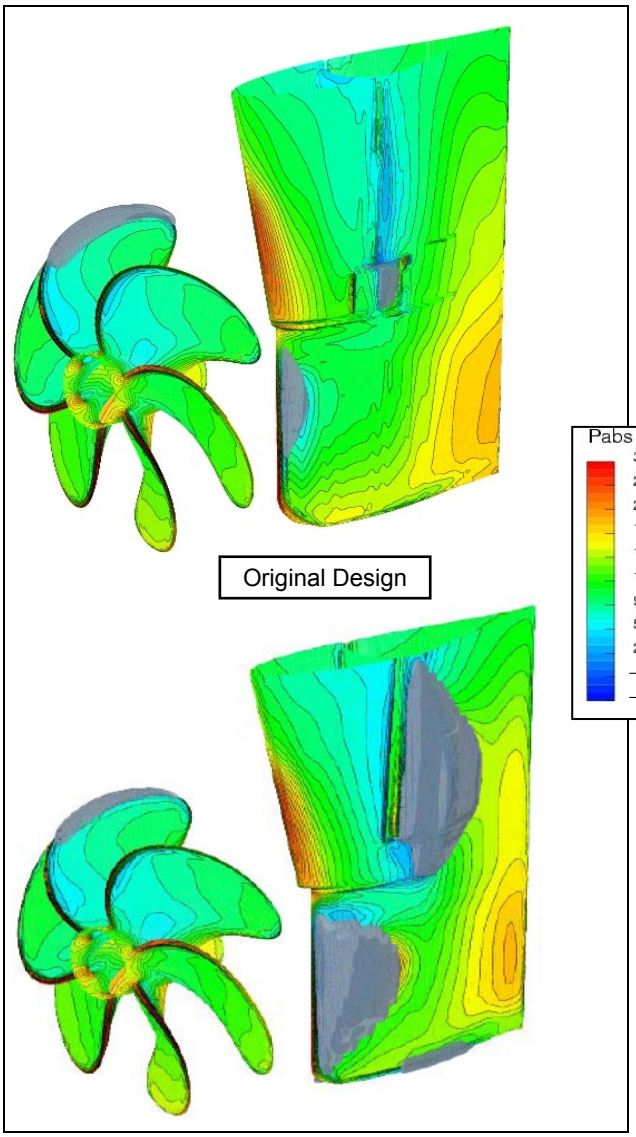

Figure 20: Pressure and cavitation (gray: iso-surface of a VoF cav-concentration of 0.01) distribution for original rudder design at 5° (top) and 10° (bottom) rudder angle

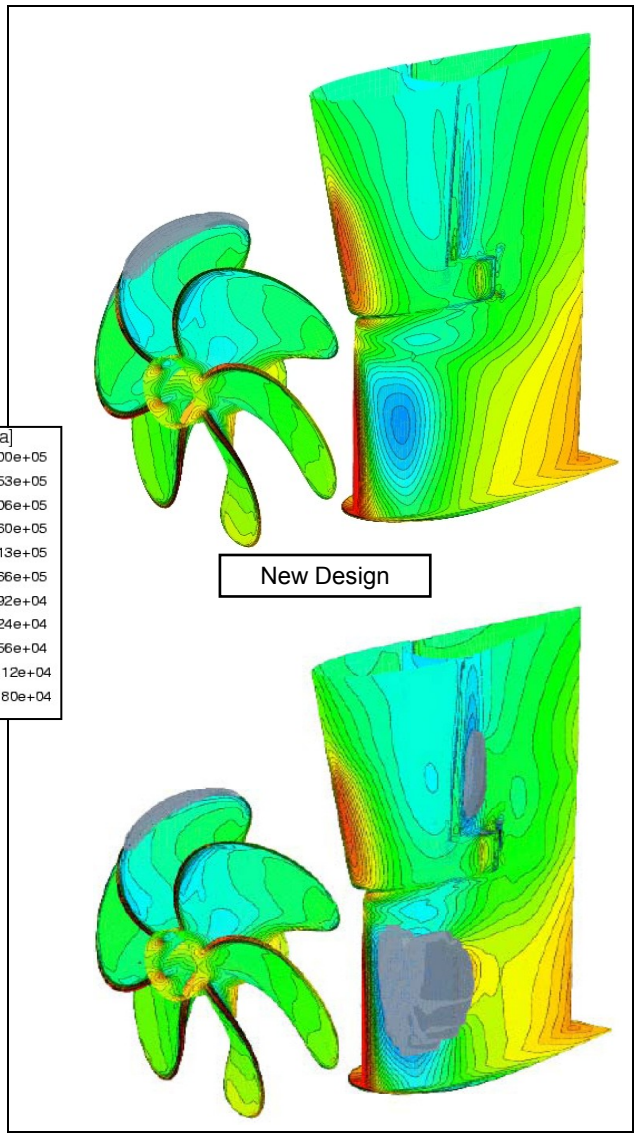

Figure 22: Pressure and cavitation (gray: iso-surface of a VoF cav-concentration of 0.01) distribution at the new rudder design at 5° (top) and 10° (bottom) rudder angle

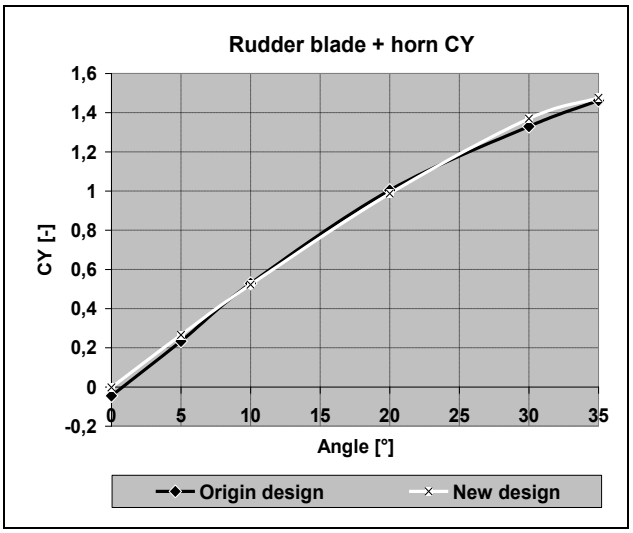

Figure 21: Transverse force coefficient of original and new rudder design

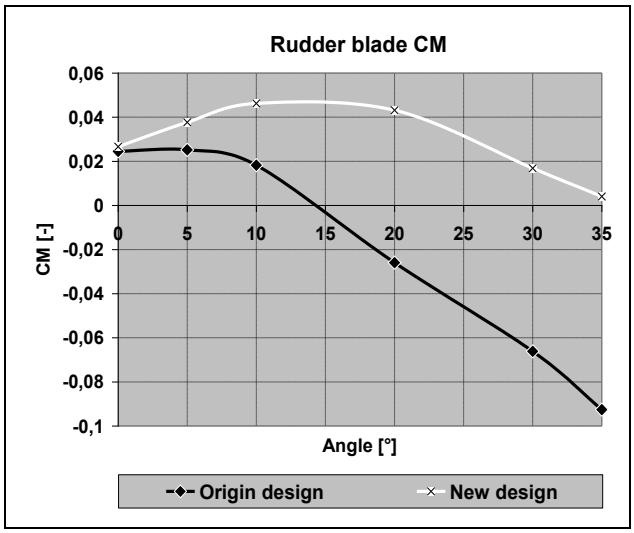

Figure 23: Rudder stock moment coefficient of original and new design